Journal of Sustainable Development of Energy, Water and Environment Systems

http://www.sdewes.org/jsdewes

Year 2026, Volume 14, Issue 3, 1140704

Original Research Article

Seawater Intrusion in Estuary Rivers: A Proposed Hydrodynamic Solution

Qais Hatem Al-Madhlom*[*1], Sanaa Abdulrazaq Jassim [2], Faris Sahib Alrammahi[3]

[1]Department of Automobile Engineering, Faculty of Engineering/ Al-Musayab, University of Babylon, Hilla, Iraq

[2]Department of Energy & Renewable Energy Engineering, Faculty of Engineering/ Al-Musayab, University of Babylon, Hilla, Iraq

[3]Department of Engineering, Imam Al-Kadhim College, Baghdad, Iraq

e-mail: met.qais.hatem@uobabylon.edu.iq, met.sanaa.abd@uobabylon.edu.iq, farisali@iku.edu.iq

Cite as: Al-Madhlom, Q.H., Jassim, S.A., Alrammahi, F.S., Seawater Intrusion in Estuary Rivers: A Proposed Hydrodynamic Solution, J.sustain. dev. energy water environ. syst., 14(3), 1140704, 2026,
DOI: https://doi.org/10.13044/j.sdewes.d14.0704

ABSTRACT

A considerable threat facing both estuary rivers and aquifers is seawater intrusion. Published articles emphasise modelling the intrusion, either mathematically or numerically, using software that lacks the capacity to introduce a hydrodynamic solution to mitigate the intrusion into fresh water. This paper presents a proposed solution for seawater intrusion using contractions. COMSOL software was used to simulate the intrusion into a hypothetical 10 km-long, 1 km-wide canal with an 80% contraction ratio. The simulation used three different conditions across four different contraction geometries, in addition to a default canal. The results show that the best geometries are the double semicircles and the wide contraction. For a 10 km canal length, the range of 10%–20% of the effective concentration will only intrude for just 0.75 km beyond the contraction.

KEYWORDS

Seawater intrusion, Estuary rivers, COMSOL software, Contraction, Saltwater intrusion, Mass transfer.

INTRODUCTION

A major challenge facing estuarine regions worldwide is seawater intrusion (SWI). This SWI challenge threatens both humans and the ecological resources in estuarine regions [1], [2]. As salty water intrudes into rivers, people living in estuarine cities are forced to restrict their consumption of fresh water as much as possible [1], [3], [4]. In addition, the aquatic life in the river's freshwater will retreat upstream, while the aquatic life in the saltwater will move upstream where the seawater has recently extended into the river. This change creates an imbalance in the regional ecosystem [5], [6]. From another perspective, the influence of the intrusion is not limited to the ground surface but extends to estuarine aquifers and soil salinisation [5], [6].

In recent years, the level of SWI has increased exponentially due to climate change and upstream dam construction in rivers, resulting in reduced river discharge [1], [2].

Many published studies have examined SWI, focusing on different aspects of the field, such as the influence of reservoir operations on river discharge and, thus, on saltwater intrusion.

* Corresponding author

It can be exemplified by the study of the Changjiang River Estuary [7], which proposed an ecological operation to mitigate the intrusion. Another study considered the influence of intertidal conditions on SWI [8]. Salinity intrusion in the Modaome estuary of the Pearl River Delta [1] was investigated using Empirical Orthogonal Functions and a set of statistical techniques, based on historical data from six stations. After examining characteristic factors influencing river intrusion, the study found that runoff is the largest contributor at 40% [1]. Another study examined seawater intrusion in the Yangtze River Estuary [3] and investigated the primary factors driving it; an important finding was that intrusion varies throughout the year, being most prevalent from November to April, with the greatest range in February and March [3]. One additional study examined the influence of the severe summer and autumn 2022 drought and three typhoons on seawater intrusion in the Changjiang Estuary [4]. The intruding water affected water quality within the Qingcaosha Reservoir, resulting in unsuitable water for intake for 98 days. The paper concluded that the intrusion was caused by a combination of low river flow rate and typhoons [4]. Another study undertook a numerical simulation of seawater intrusion in the estuary of the Yangtze River; an interesting finding was that runoff was the greatest factor affecting intrusion [9]. Moreover, an investigation of SWI in the Yangtze River Estuary using the MIKE 21 model [10] concluded that the critical discharge required to withstand large-scale intrusion exceeds 10,000 m3/s [10]. Another study considered the influence of wind and waves on SWI within the Yangtze Estuary [11]. From yet another perspective, an investigation was conducted into the influence of drought conditions and tidal forces on the SWI in the Lower Chao Phraya River [12].

Regarding rivers in Vietnam, a study developed three machine learning models to predict saltwater intrusion in the Mekong estuary [13]. The three developed models are a gated recurrent unit (GRU), a GRU-SFO (sailfish optimiser algorithm), and a GRU-GWO (grey wolf optimiser). The results showed that SFO and GWO improved the GRU model's performance in predicting seawater intrusion [13]. Another study utilised a 3D hydrodynamic model (MIKE 3) to predict SWI in the Mekong Delta [14]. The results indicate that saltwater stratified at the beginning and end of the dry season, with mixing in between. The study also found that the intrusion began earlier in 2022 than in previous years [14].

Verri et al. [15] studied the influence of river discharge and sea level rise on SWI in the Po di Goro estuary, Italy. Another study examined the influence of freshwater discharge, wind, sea level, and estuary geometry on SWI in the Chao Phraya Estuary, Thailand [16]. Delft2D and Delft3D software were utilised to simulate SWI under tidal effects and different river flows in the Minho River, in Spain and Portugal [17]. The studies of SWI also extend to cover intrusion into coastal aquifers and groundwater quality. Two papers on the influence of layered well pumping on seawater intrusion in the coastal layered aquifers of the Danqing River in Liaodong Bay (China) were published in 2020 [18] and 2024 [2]. The results showed that layered intrusion is directly affected by the layered pumping flow rate. The risk of intrusion within the coastal city of Shenzhen (China) was assessed by [5]. One conclusion is that approximately 49.31 km2 of the coastal city area was affected by the intrusion. Perumal et al. [6] reviewed 94 published papers on seawater intrusion through coastal aquifers and highlighted the importance of regulatory measures to control it. Another study examined the influence of preferential flow on marine nitrates and pore-water flow in a coastal region [19] and pointed out that preferential flow has a considerable impact on groundwater flow and salinity distribution.

Three papers are noteworthy for this research. The first is the study done by Truong et al. [20]. Here, the researchers considered simulating SWI and land subsidence in the coastal aquifers of the Pingtung Plain, Taiwan. COMSOL Multiphysics was employed to simulate a 2D hydraulic-mechanical-chemical model. The study explored the locations of proposed production and injection wells to mitigate SWI. In the second paper, Missimer and Maliva [21] explored 11 hydrodynamic barriers, including injection and abstraction wells, to mitigate SWI in coastal aquifers. The third key study was conducted by Hendrickx et al. [22], who explored

SWI mitigation in the Lower Mississippi River near New Orleans, United States, and proposed and examined the influence of an earthen sill to mitigate the intrusion. The distinguishing feature of these three works is that they proposed hydrodynamic solutions to mitigate SWI in a freshwater river.

Overall, existing research in this field has chiefly focused on simulating or modelling seawater intrusion in estuarine rivers without proposing a hydrodynamic solution. By contrast, studies proposing solutions to this problem are notably scarce.

To address the aforementioned research gaps, this study proposes a hydrodynamic method that could be a solution (given suitable conditions) for SWI in estuarine rivers. To introduce the solution, this article considers a hypothetical canal (10 km long) and uses COMSOL software for simulation. Since the paper focuses on introducing a proposed solution, a hypothetical canal is used for simulation; thus, this solution can be used in the future if substantiated.

The innovation of this paper is the use of contraction to mitigate seawater intrusion. The objectives of this paper are to answer the following questions:

- How can SWI be minimised in an estuary river?
- What is the best form of riverbed contraction to offer the best solution?
- How much could upstream SWI be mitigated compared to the downstream of the river when using contraction?

MATERIALS AND METHODS

To mitigate SWI in an estuary river, this paper proposes a hydrodynamic solution that reduces the waterway's cross-sectional area. To explore the effectiveness of this solution, a hypothetical 10 km canal is proposed for simulation. The simulation was undertaken using COMSOL software. Additionally, to explore the influence of contraction shape on the intrusion, different contraction geometries were used in the simulation.

Mathematical Models

Two sets of governing equations are involved in the SWI problem. The first set regards the general fluid flow (including open channel), while the second set regards mass transfer, or more specifically, equations of diluted species transport. The first set of equations involves equations of continuity and momentum, eq. (1) and eq. (2). These two equations can be written as follows [23], [24], [25]:

$$\frac{\partial \rho}{\partial t} + \nabla \cdot (\rho u) = 0 \tag{1}$$

$$\rho \frac{\partial u}{\partial t} + \rho(u \cdot \nabla)u = \nabla \cdot [-p + \tau] + \rho a \tag{2}$$

The second set of equations describes the transport of diluted species. Transport occurs due to two phenomena: diffusion and convection. The effect of these two phenomena is formulated by the following equations [23], [25]:

$$\frac{\partial c_i}{\partial t} + \nabla \cdot J_i + u \cdot \nabla c_i = R_i \tag{3}$$

$$J_i = -D \nabla c_i \tag{4}$$

The second term of eq. (3) represents the diffusion effect, while the third term represents convection. Diffusion occurs from a high concentration to a low one, while convection occurs due to the bulk movement of a mass of solvent. Therefore, in the case of saltwater intrusion in an estuary river, the two phenomena are opposite in action to each other. Hence, convection can be increased by minimising the cross-sectional area of a watercourse.

Validation

A physical model was prepared in the lab to verify the software simulation. The model consists of a 1-metre-long canal with a 10 cm width connecting two basins of dimensions 30 cm × 30 cm × 30 cm (**Figure 1a** and Appendix **Figure A1**). One basin represents the upstream source of fresh water, while the second one represents the saltwater of the sea. The flow rate within the canal is maintained at a flow velocity of 0.005 m/s from the fresh basin to the saltwater basin. It was achieved by allowing fresh water from a tap to flow into the fresh basin and, in turn, into the saltwater basin through the canal. The flow conditions are balanced by letting the water flow out of the saltwater basin through the system's drain (Appendix **Figure A1**). The inlet and outlet flows are both controlled by using ball valves (**Figure 1a**). To maintain the salinity at a seawater level of 35000 ppm, saltwater is continuously added to the saltwater basin. A submersible pump is placed in the salt basin to mix the water and achieve a homogeneous solution (**Figure 1a**). After initiating the experiment, salinity readings are continuously taken at five points along the canal, with point 1 near the freshwater basin and point 5 near the saline-water basin.

Two experiments were conducted using the physical model, the first without a triangle contraction (**Figure 1a**), and the second with a triangle contraction (**Figure 1b** and Appendix **Figure A2**).

The corresponding numerical models (without and with triangle contraction) were built in COMSOL, with all boundaries set as in the physical model. The results from the numerical model are compared with those from the physical one for the two cases (**Figure 1c** and **Figure 1d**). The results of the two comparisons show that the concentration from the physical modelling is slightly lower than that from the software modelling. Still, this difference can be explained by the low mixing of saline water with the fresh water within the canal (**Figure A3**).

Simulation

COMSOL software was used to develop a 2D model for SWI simulation. The simulation can be summarised as follows:

Physics and geometry. Two interfaces were used integrally to simulate SWI. They are: Shallow Water Equation SWE, and Transport of Diluted Species TDS. As mentioned before, different geometries were used to explore the influence of the contraction shape on SWI. The geometries tested in this article are: triangle (see **Figure 2b** and **Figure A4**), semicircle (see **Figure 2c** and **Figure A5**), double semicircles (see **Figure 2e** and **Figure A6**), and wide contraction (see **Figure 2e** and **Figure A7**). The length and the width of the geometries are 10 km and 1 km, respectively. Except for the geometries in Appendix **Figure A4**, **Figure A5**, **Figure A6**, and **Figure A7**, which are tested under an additional 5 km canal length between the outlet and the contraction, all the contractions have a dimension of 0.4 km from one side; thus, the net width of the waterway is 0.2 km at the contraction. Each of these geometries was tested at two flow velocities (0.5 m/s and 1 m/s), and compared with a canal without a contraction (see **Figure 2a**). In addition, each geometry was tested under conditions such that it was 5 km from the sea mouth (see **Figure A4**, **Figure A5**, **Figure A6**, and **Figure A7**).

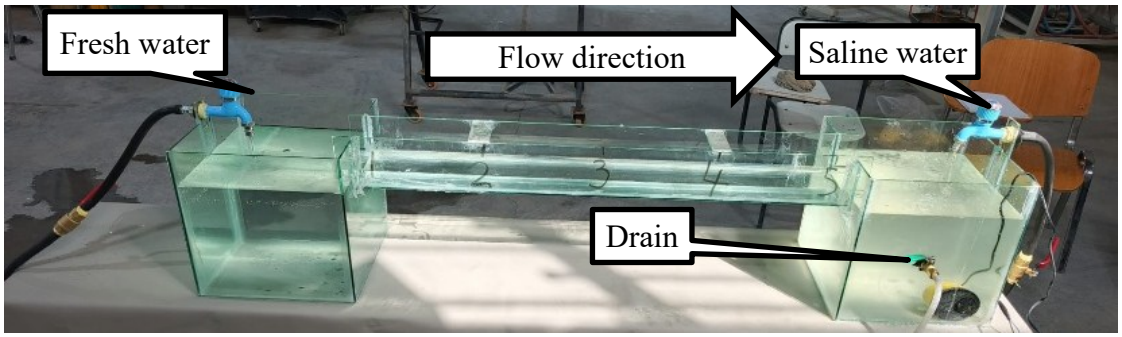

(a)

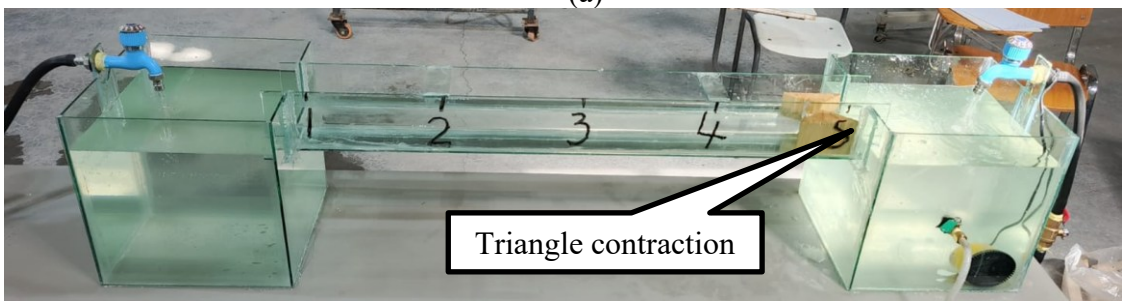

(b)

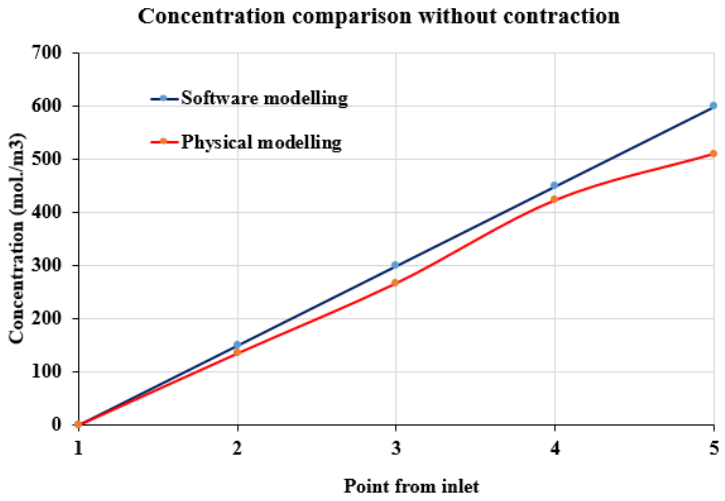

(c)

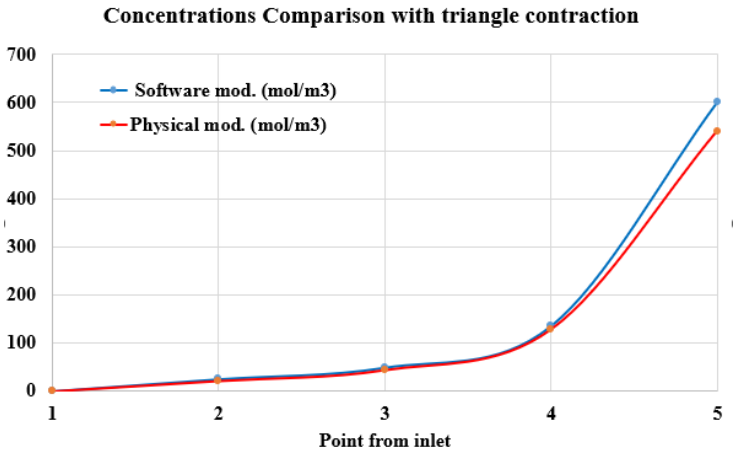

(d)

Figure 1. Physical modelling of the intrusion: real model without triangle contraction (a); real model with triangle contraction (b); comparison between the software and physical modelling of concentration without contraction (c); comparison with contraction (d)

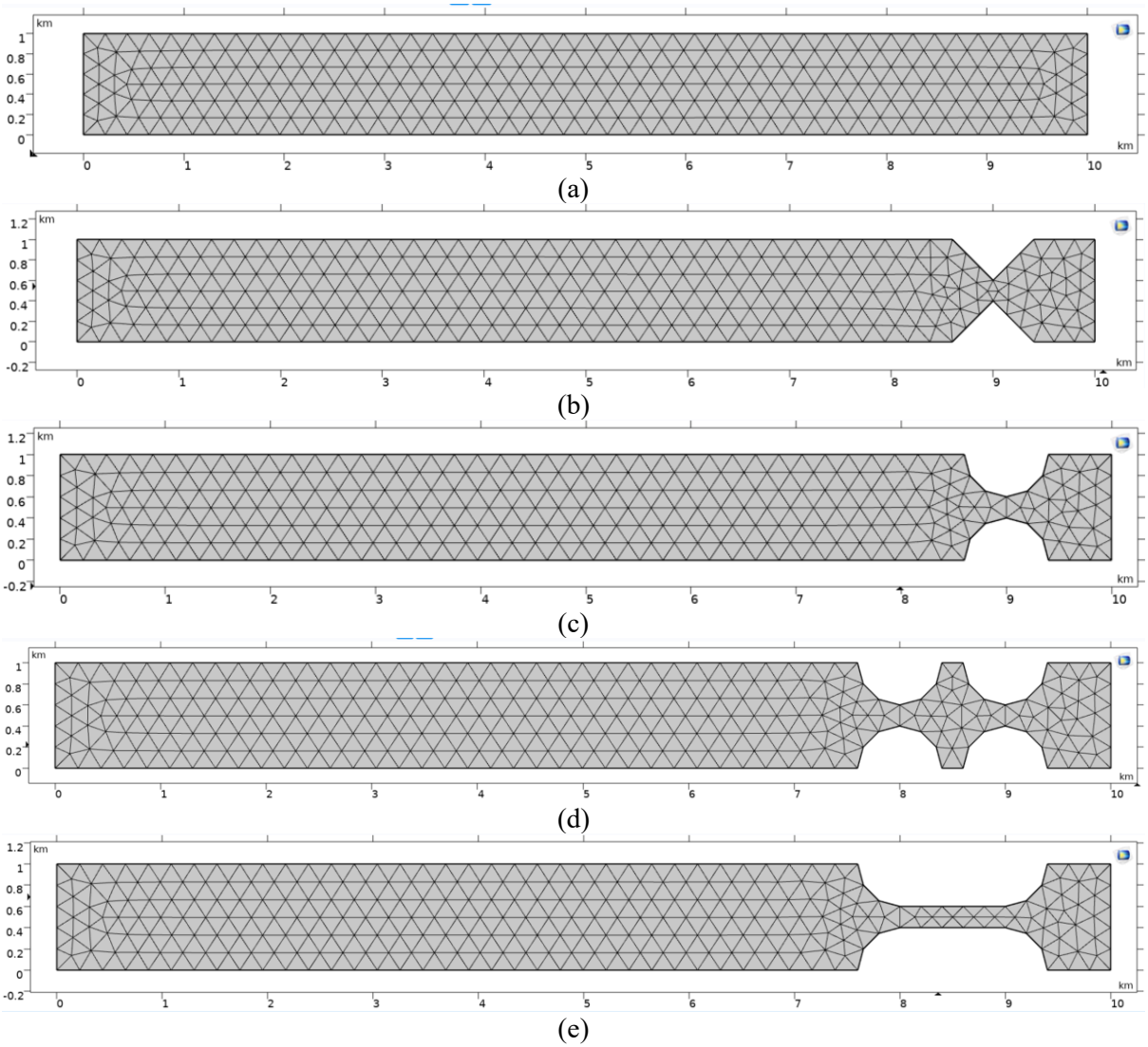

Figure 2.Geometries of contractions after meshing: default canal (a); triangle contraction (b); semicircle contraction (c); double semicircles contraction (d); wide contraction (e)

Boundary conditions and initial values, and meshing. For each model, the initial values and boundary conditions were as follows. At the shallow water equation interface, the initial values for the water depth and velocity were 1 m and 0.5 m/s, respectively. For the boundary conditions for the inlet and outlet velocity, the Vi & Vo were 0.5 m/s. To examine the influence of convection, the intrusion was also investigated with Vi & Vo of 1 m/s. The default meshing settings were used to generate the mesh for each canal geometry (see **Figure 2**). There are software defaults to a physically controlled mesh for the sequence type, and this choice was used for the meshing process.

Scenarios. Three different scenarios were used in the simulation. The first one is at 0.5 m/s for the inlet and outlet velocity. The second one is at 1.0 m/s for the inlet and outlet velocity, while the third is at 0.5 m/s for the inlet and outlet velocity and a 5 km extension between the sea-mouth and centre of contraction. For all scenarios, the boundary conditions for the inlet and outlet were set to 0 mol/m^3 and 600 mol/m^3, respectively. For all runs, the diffusion coefficient (D) was assumed to be 1 m^2/s, instead of the actual value of 1×10^{-9} m^2/s. There are three reasons behind this assumption:

- To increase the diffusion effect, since the actual value produces an unrecognisable change in the salinity of the water of the canal. To explain the differences between the two values of the D, consider **Figure 3a**, where the saltwater intrusion is limited to a

very short length of the canal due to utilising D equal to 1×10^{-9} m^2/s, compared to Figure 3b, where the intrusion is clear due to using D equal to 1 m^2/s.

- The real value of D for a model length of 10 km would result in a very short intrusion in the tail of the canal, making it very difficult to observe. Overcoming this problem requires a very long model that simulates the river's actual length, which could reach 500 km. This approach would make the model very long and very thin, and it would be difficult to present in a figure within the manuscript.
- One of the main objectives of this manuscript is to introduce the influence of contraction on the seawater intrusion within the river. Thus, two groups of figures are presented in the manuscript: the first is without contraction and the second with contraction. The same diffusion coefficient of 1 m^2/s was assumed in both cases to exaggerate the influence of seawater intrusion and clarify the differences between them.

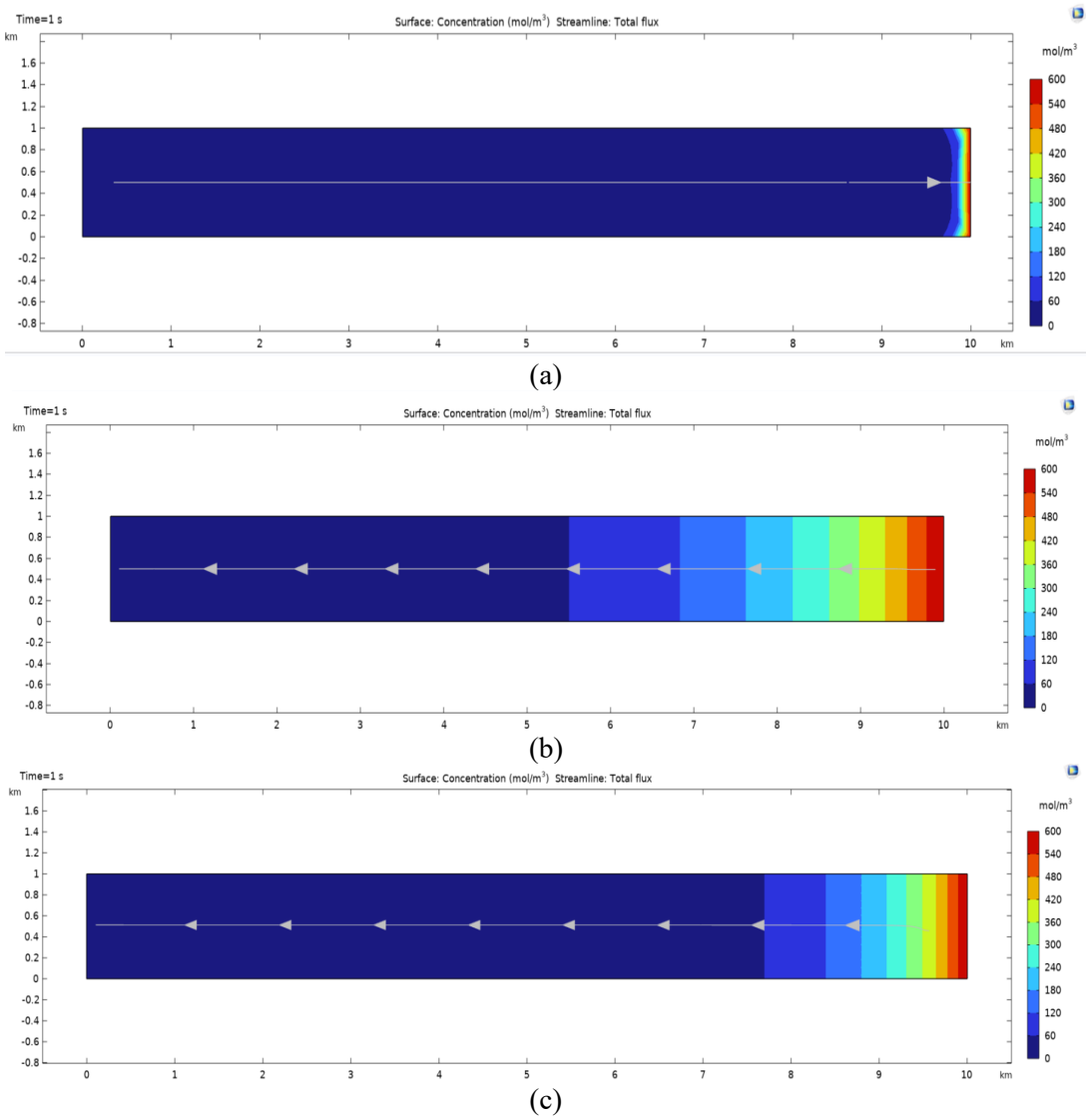

Figure 3. Seawater intrusion under default geometry and conditions: Vi & Vo of 0.5 m/s and D of 1×10^{-9} m^2/s (a); Vi & Vo of 0.5 m/s and D of 1 m^2/s (b); Vi & Vo of 1 m/s and D of 1 m^2/s (c)

RESULTS

The model was run for the geometry shown in Figure 2a, with D of 1×10-9 m2/s and Vi & Vo of 0.5 m/s. The result is shown in Figure 3a; it does not include a considerable change in concentration due to the small value of D, which produces only a short intrusion of saltwater in

the direction upstream of the sea mouth, as referred to in the Scenarios subsection. To maximise the influence of SWI, D is set to 1 m2/s; the corresponding result is shown in **Figure 3b**. From another perspective, to introduce the influence of convection, Vi & Vo were also set to 1 m/s for both. The resultant intrusion is shown in **Figure 3c**.

To explore the influence of triangular contraction, COMSOL was run under the conditions of D of 1 m2/s, and Vi & Vo of 0.5 m/s. The resultant intrusion is shown in **Figure 4a**. The influence of the contraction is clear, and the intrusion is less than the intrusion in the default canal (without contraction, **Figure 3b**). Then, the model was run under Vi & Vo of 1 m/s to explore the influence of flow velocity (**Figure 4b**). At this velocity, the intrusion length decreases compared with the 0.5 m/s flow velocity condition (**Figure 4a**), indicating the significance of flow velocity in mitigating the intrusion. The triangle contraction was also tested under an extension of 5 km between the outlet and the contraction, with Vi & Vo set to 0.5 m/s. The resultant intrusion is shown in **Figure 4c**, with the extension amplifying the contraction's influence, causing a very short intrusion behind it. This points to an effective way to increase the contraction's influence.

Other geometries were tested under the same conditions; thus: 1) 0.5 m/s Vi & Vo, 2) 1 m/s Vi & Vo; and 3) 5 km extension and 0.5 m/s velocity, with D of 1 m2/s for all cases. The resultant intrusions for each case are shown in **Figure 5** to **Figure 7**, which indicate the influence of each contraction on the length of intrusion. The effects of contractions can be enhanced by using extensions, which will decrease the length of the intrusion.

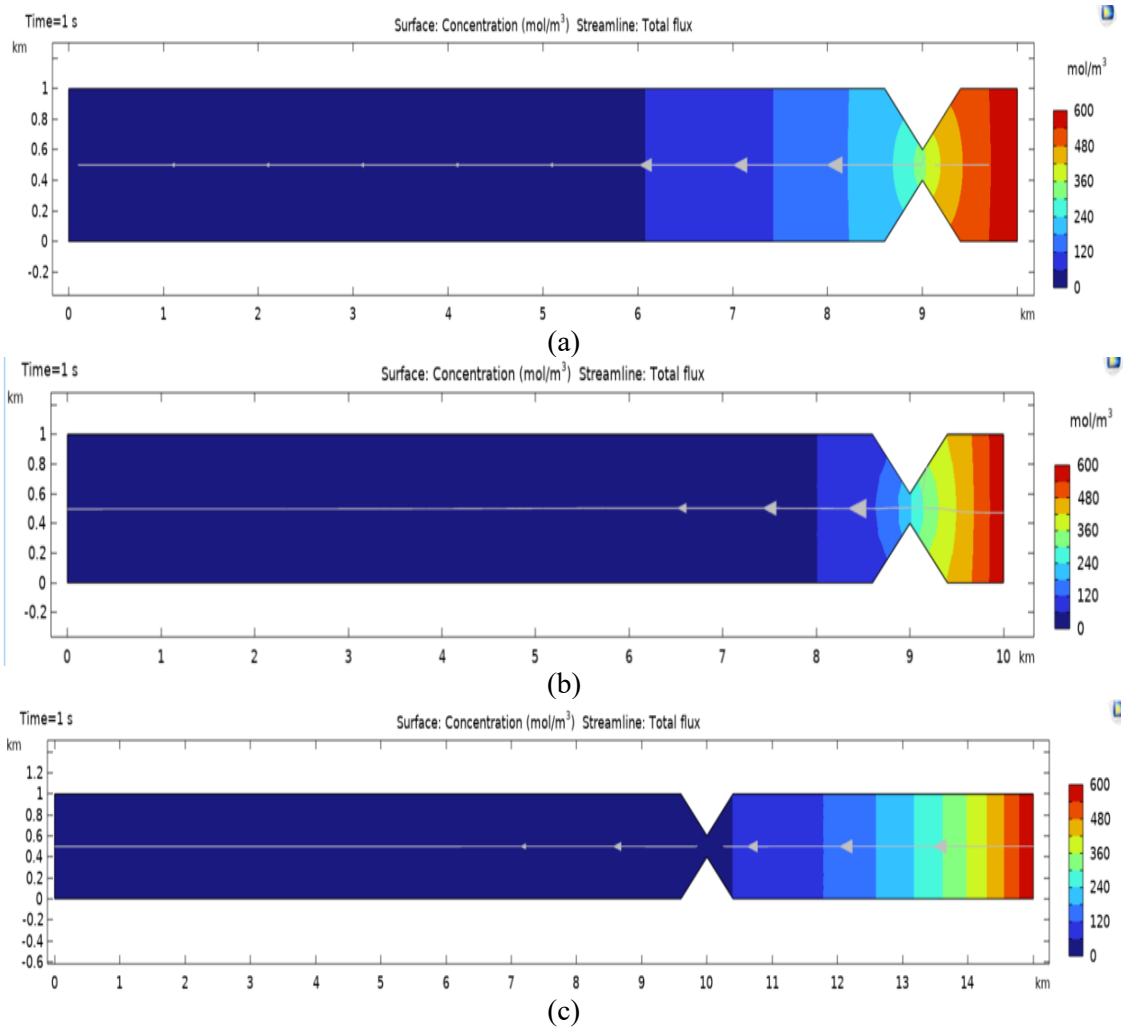

Figure 4. Seawater intrusion under triangle geometry and conditions: Vi & Vo of 0.5 m/s and D of 1 m^2/s (a); Vi & Vo of 1 m/s and D of 1 m^2/s (b); (c) with extension and Vi & Vo of 0.5 m/s and D of 1 m^2/s

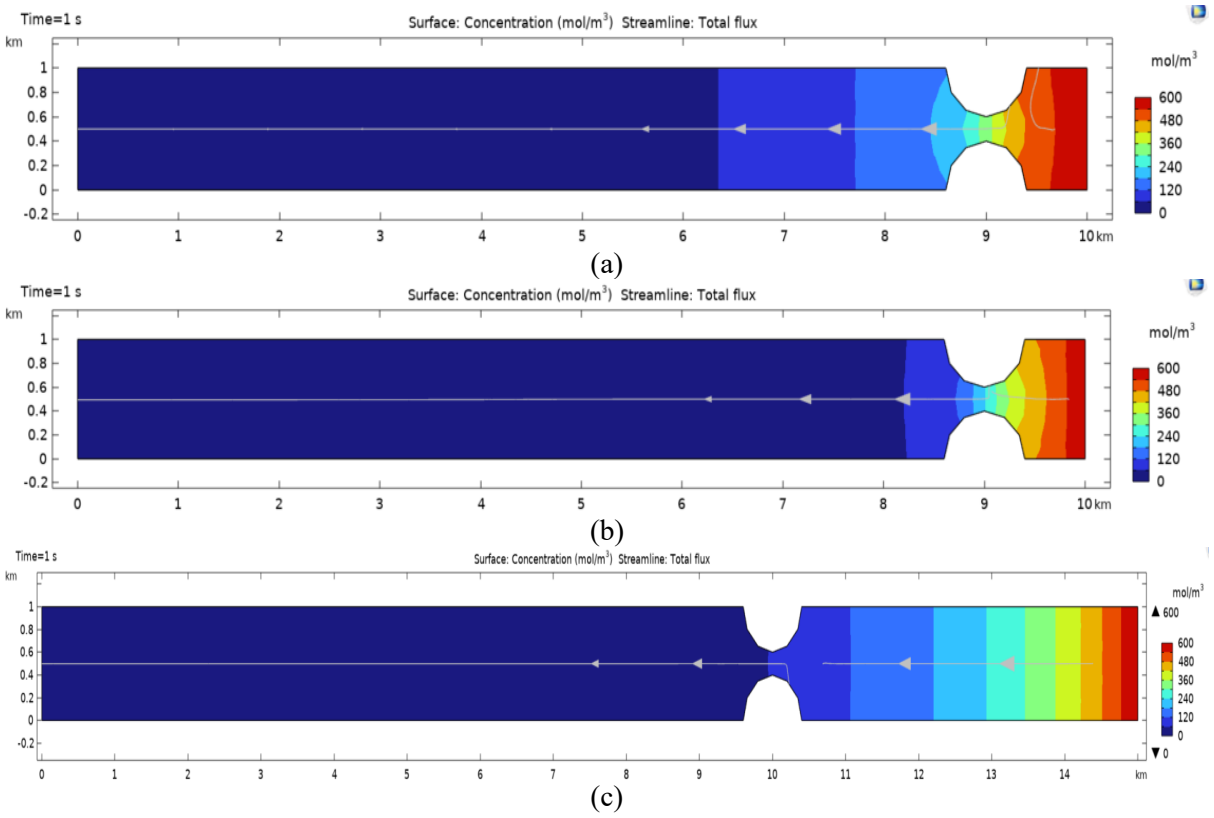

Figure 5. Seawater intrusion under semicircle geometry and conditions: Vi & Vo of 0.5 m/s and D of 1 m^2/s (a); Vi & Vo of 1 m/s and D of 1 m^2/s (b); with extension and Vi & Vo of 0.5 m/s and D of 1 m^2/s (c)

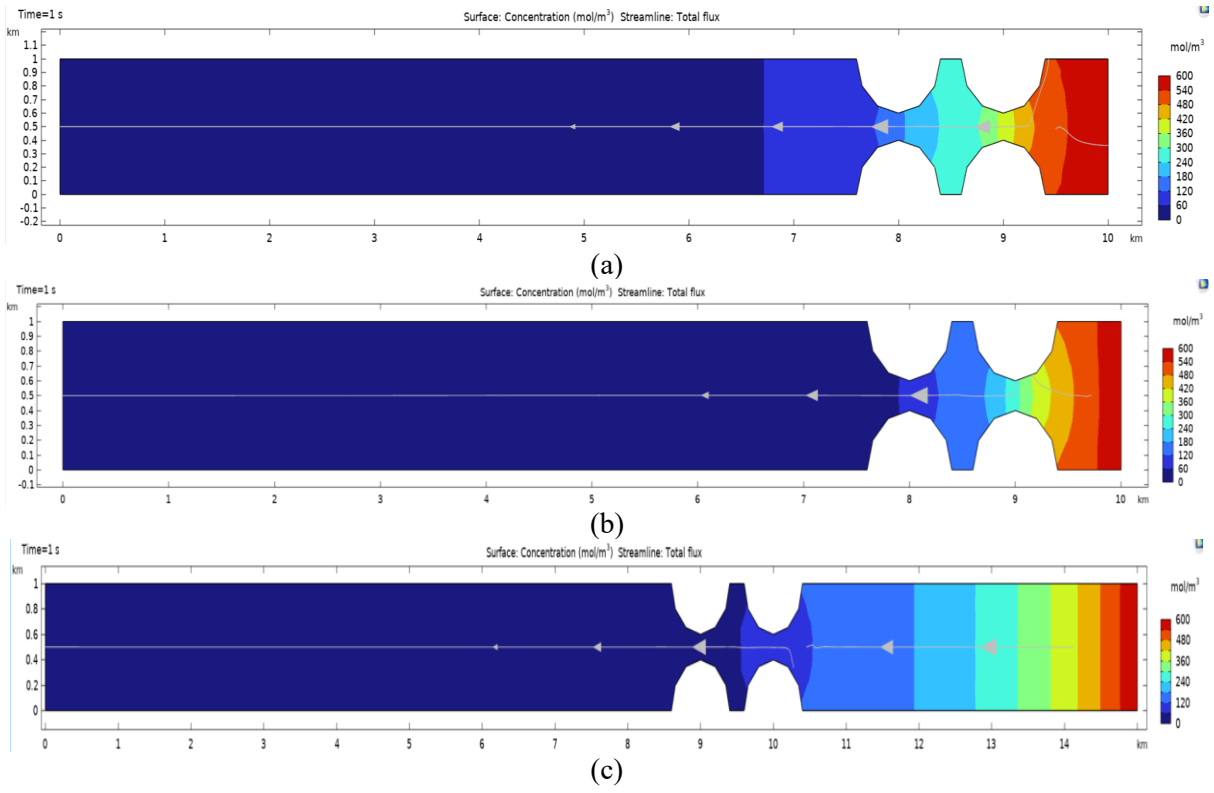

Figure 6. Seawater intrusion under double semicircles geometry and conditions: Vi & Vo of 0.5 m/s and D of 1 m^2/s (a); Vi & Vo of 1 m/s and D of 1 m^2/s (b); with extension and Vi & Vo of 0.5 m/s and D of 1 m^2/s (c)

From a comparison between the different geometries under the conditions of Vi & Vo of 0.5 m/s, and D of 1 m2/s (**Figure 3b**, **Figure 4a**, **Figure 5a**, **Figure 6a**, and **Figure 7a**), it can be found that the best geometry that results in the least intrusion is double semicircles (**Figure 5a**). Since the range of intrusion (60–120 mol/m3) is limited to about 0.75 km beyond the contraction, whereas the other geometries extend beyond that limit. The reason is that the presence of the first contraction (the one closer to the downstream end) creates a high-velocity region (stronger convection) that helps prevent the saline tongue from penetrating the space between the two semicircles. While this space helps mitigate saltwater intrusion, the second semicircle contraction aims to prevent saline water from advancing upstream.

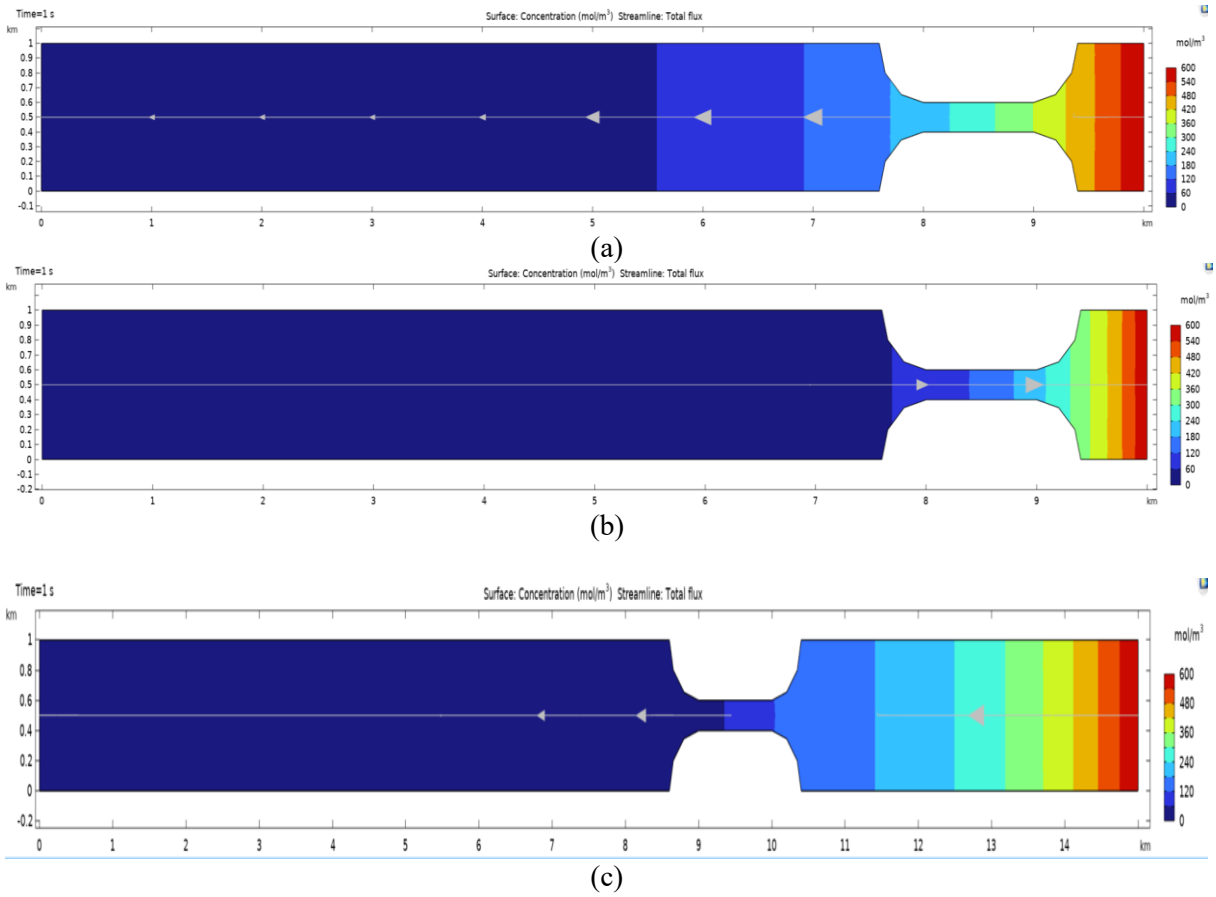

Figure 7. Seawater intrusion under wide contraction geometry and conditions: Vi & Vo of 0.5 m/s and D of 1 m^2/s (a); Vi & Vo of 1 m/s and D of 1 m^2/s (b); with extension and Vi & Vo of 0.5 m/s and D of 1 m^2/s (c)

In another comparison between the geometries under 1 m/s Vi & Vo, and 1 m/s2 for D (**Figure 3c**, **Figure 4b**, **Figure 5b**, **Figure 6b**, and **Figure 7b**), it can be seen that the best geometries that result in the least intrusion are double semicircles and a wide contraction (**Figure 6b** and **Figure 7b**). The reason may be that the velocity increases during these contractions compared to other types, boosting convection and diluting the intrusion. These two geometries result in close intrusions within the canal. Also, double semicircles and a wide contraction both produce the least intrusion for the 5 km extension geometries (**Figure 6c** and **Figure 7c**).

DISCUSSION

From examining **Figure 3** to **Figure 7**, the intrusion length is inversely proportional to the river flow velocity. Given the relationship between velocity and intrusion length, many studies have indicated a link between saltwater intrusion and river discharge; some of these studies are listed below. According to the research on the Sumjin River Estuary, intrusion is strongly influenced by discharge. The results indicated a power function between the river discharge and the distance of saltwater intrusion [26]. Another study found a strong correlation between flow rate and saltwater concentration in the north and south branches of the Yangtze River Estuary. Also, it highlighted the significant role of river discharge in determining salinity levels within rivers [25]. Yet another study stated that the stratification and saltwater wedge estuary of the Magdalena River (Colombia) are mainly driven by the river's discharge [27]. These published articles concluded that the river discharge strongly influences the length of the intruding saltwater, and that the relationship between them is inversely proportional. Since the discharge of the river is the product of cross-sectional area by the velocity of the flow, it could be surmised that the length of intrusion is inversely proportional to the velocity of the river flow. This fact agrees with the results of the current study.

Based on the results, the best geometries for mitigating SWI among the proposed geometries are the double semicircle and the wide contraction. To explain the reasons, the figures showing the velocity (**Figure 8**, **Figure 10**, **Figure 12**, and **Figure 14**) and the height of the free water surface (**Figure 9**, **Figure 11**, **Figure 13**, and **Figure 15**) for each geometry are obtained from the software.

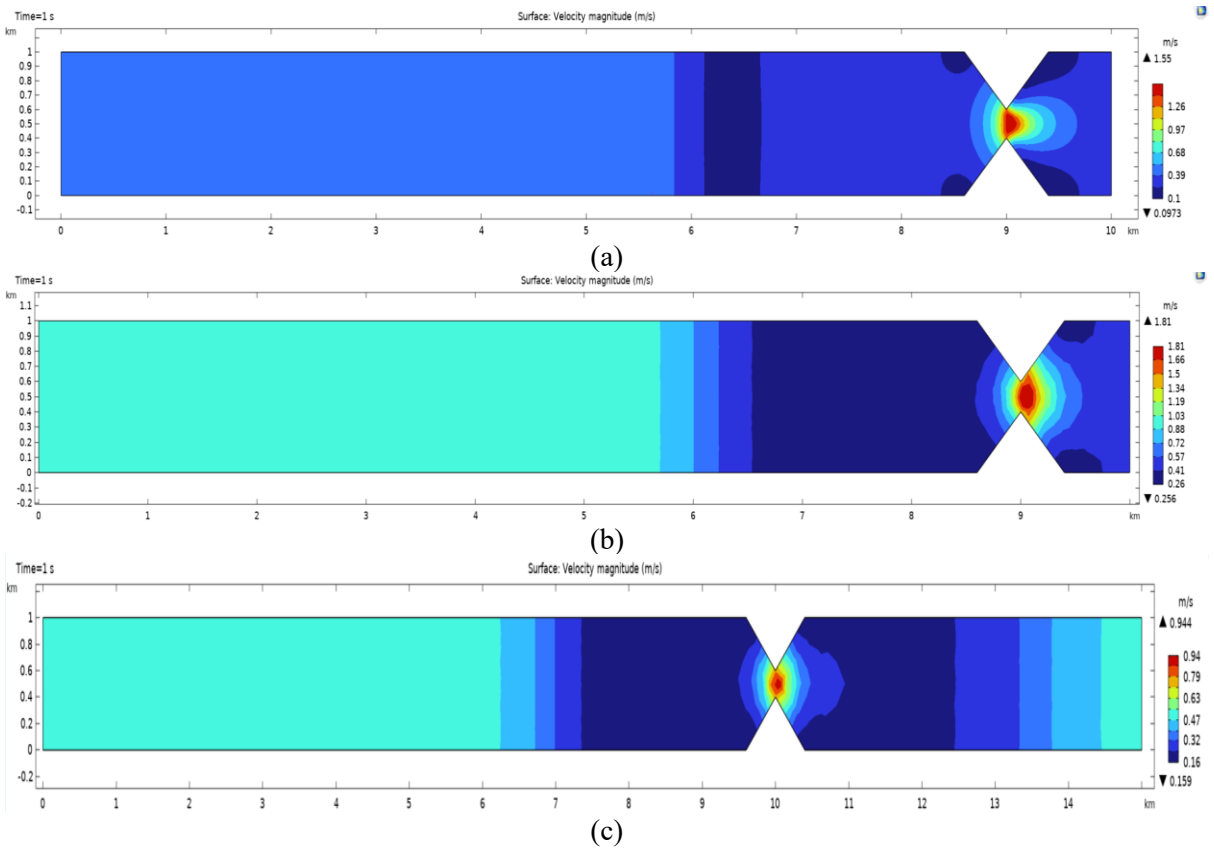

Figure 8. Velocity distribution for triangle geometries: Vi & Vo of 0.5 m/s and D of 1 m^2/s (a); Vi & Vo of 1 m/s and D of 1 m^2/s (b); with extension and Vi & Vo of 0.5 m/s and D of 1 m^2/s (c)

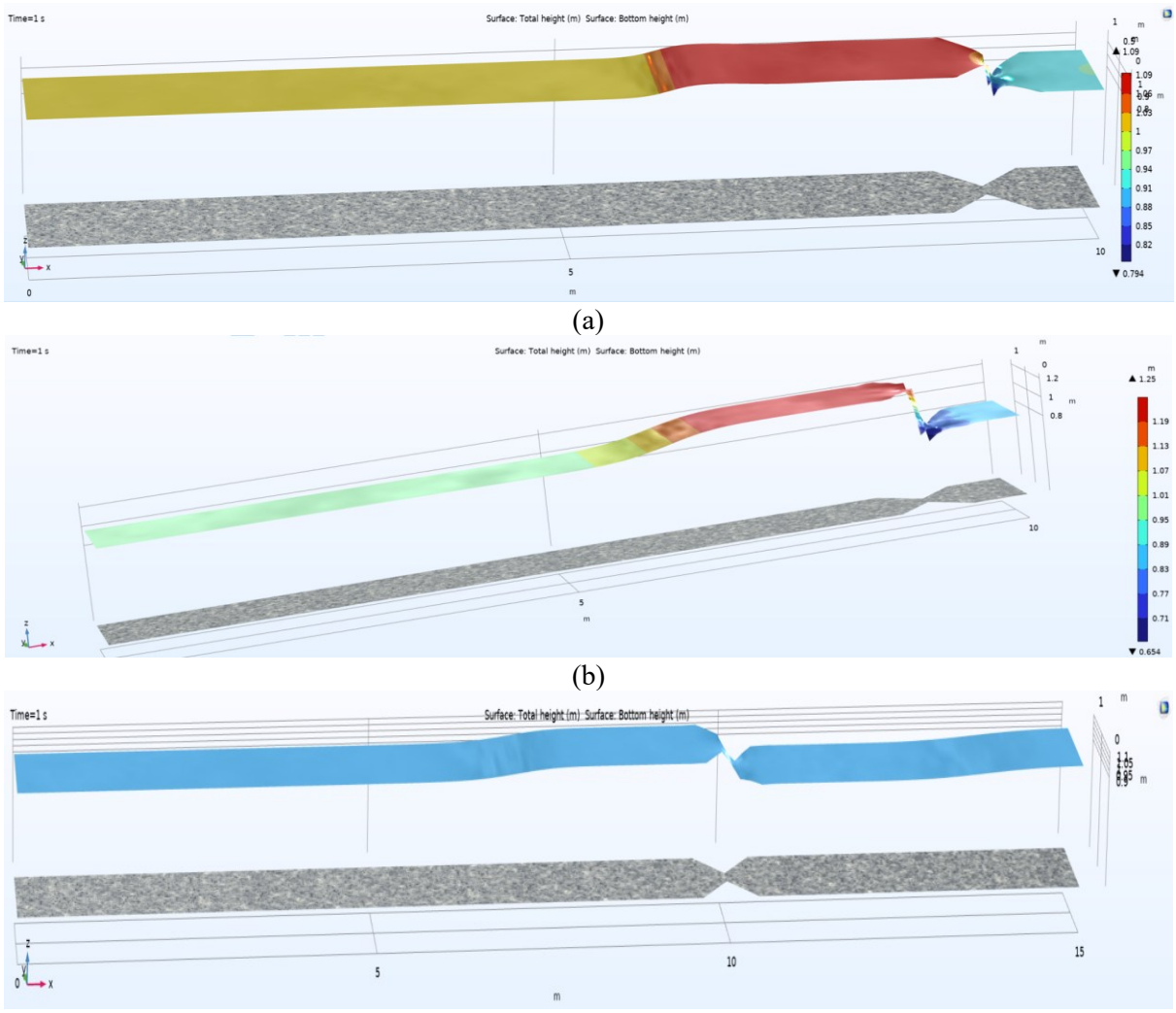

(a)

(b)

(c)

Figure 9. Height of free water surface for triangle geometries: Vi & Vo of 0.5 m/s and D of 1 m^2/s (a); Vi & Vo of 1 m/s and D of 1 m^2/s (b); with extension and Vi & Vo of 0.5 m/s and D of 1 m^2/s (c)

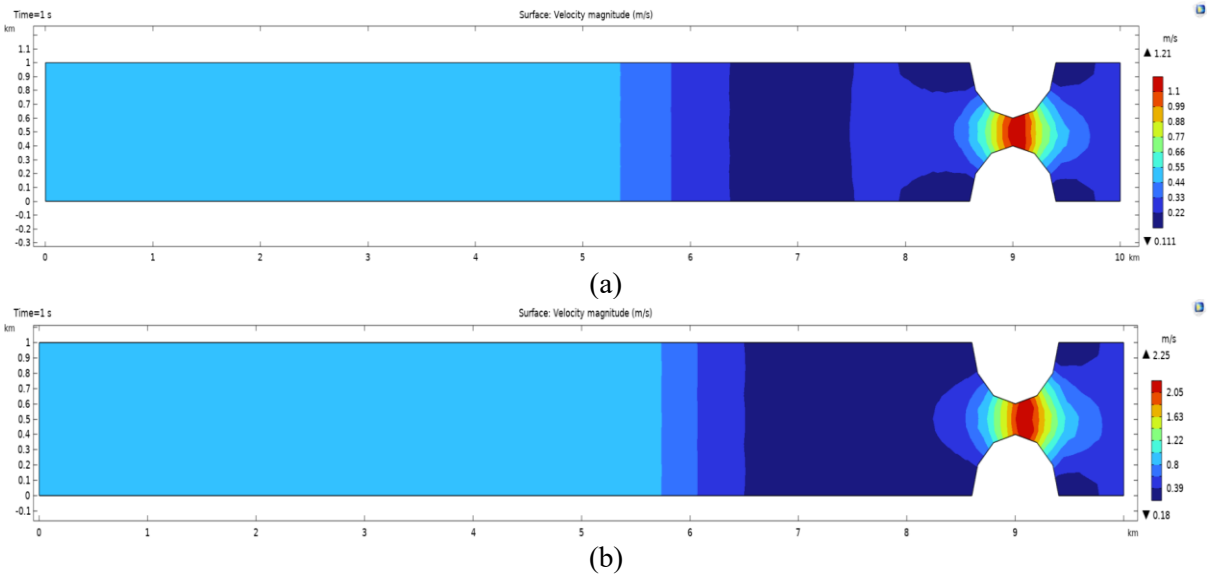

(a)

(b)

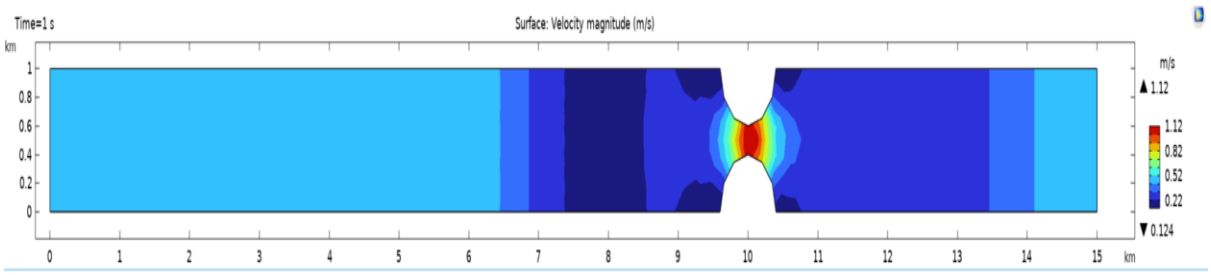

(c)

Figure 10. Velocity distribution for semicircle geometries: Vi & Vo of 0.5 m/s and D of 1 m^2/s (a); Vi & Vo of 1 m/s and D of 1 m^2/s (b); With extension and Vi & Vo of 0.5 m/s and D of 1 m^2/s (c)

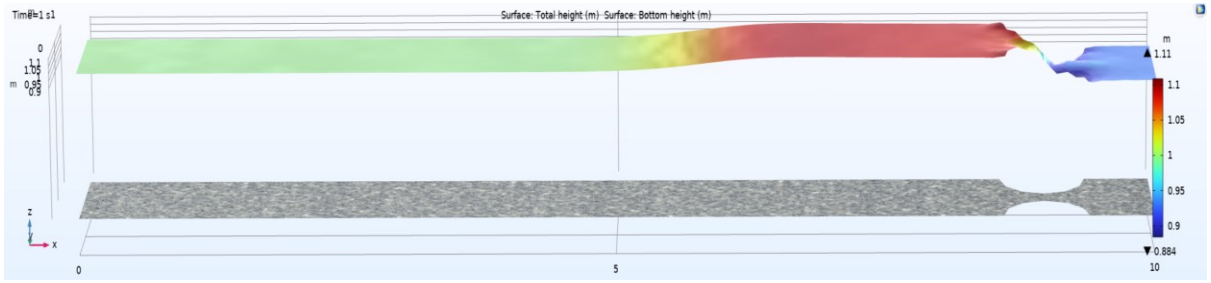

(a)

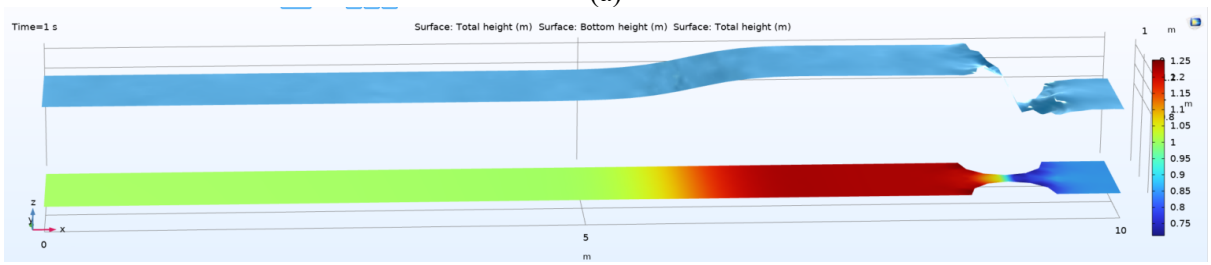

(b)

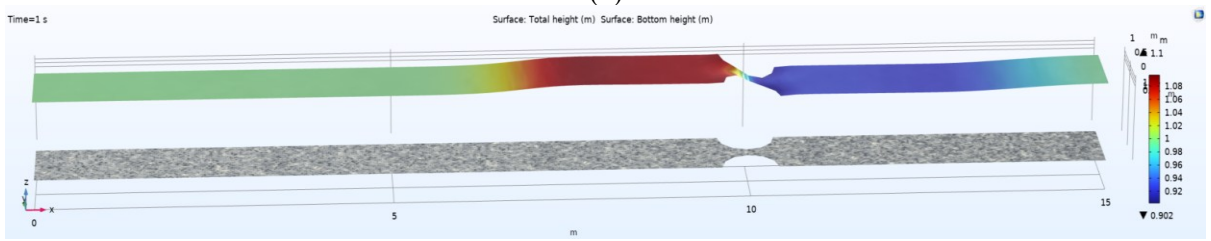

(c)

Figure 11. Height of free water surface for semicircle geometries: Vi & Vo of 0.5 m/s and D of 1 m^2/s (a); Vi & Vo of 1 m/s and D of 1 m^2/s (b); with extension and Vi & Vo of 0.5 m/s and D of 1 m^2/s (c)

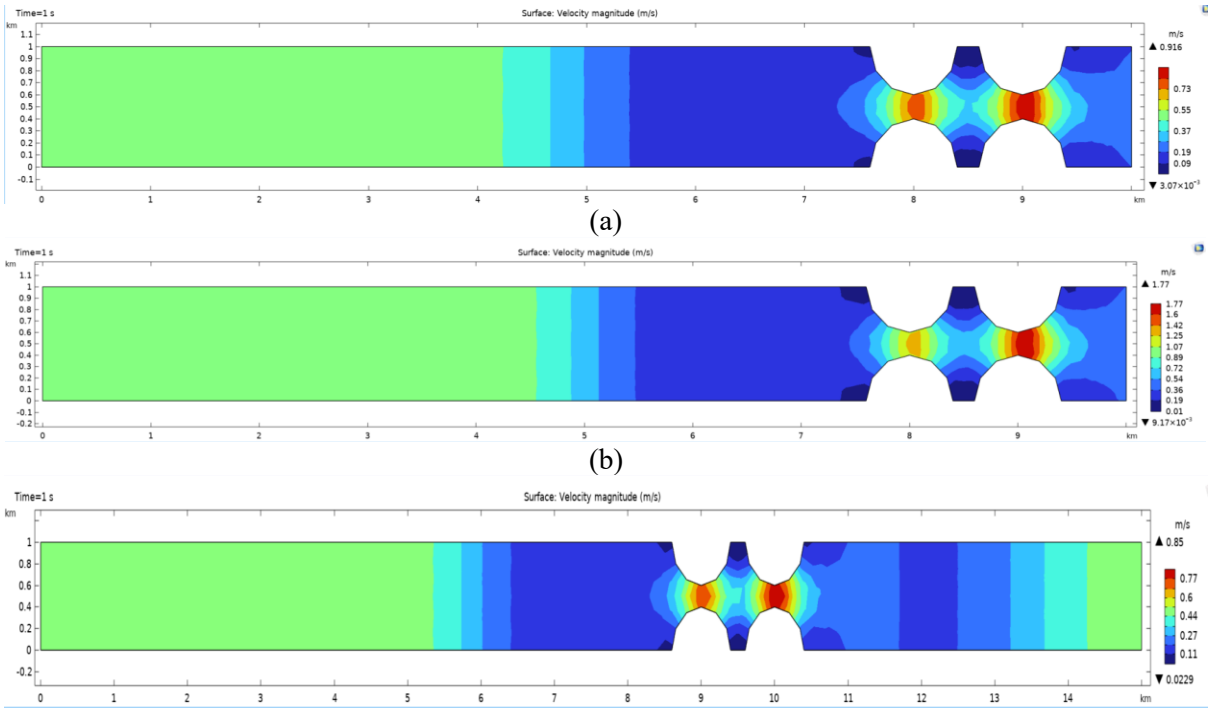

Figure 12. Velocity distribution for semicircle geometry: Vi & Vo of 0.5 m/s and D of 1 m^2/s (a); Vi & Vo of 1 m/s and D of 1 m^2/s (b); with extension and Vi & Vo of 0.5 m/s and D of 1 m^2/s (c)

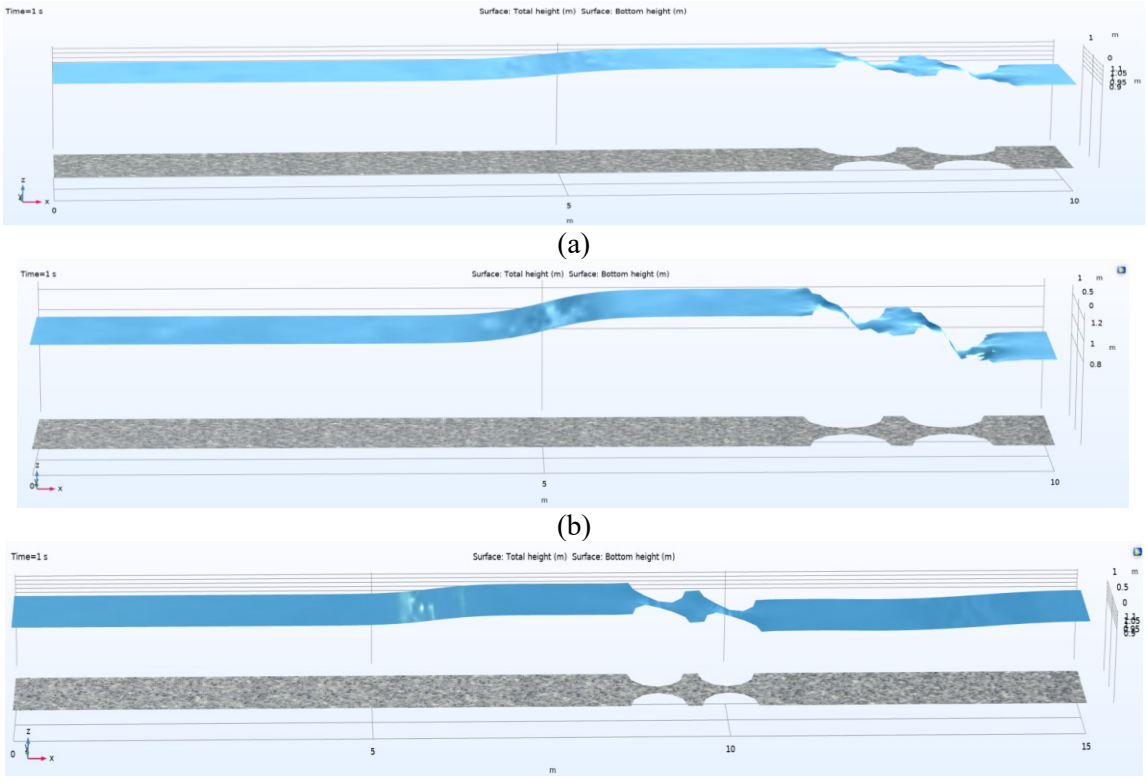

Figure 13. Height of free water surface for double semicircles geometry: Vi & Vo of 0.5 m/s and D of 1 m^2/s (a); Vi & Vo of 1 m/s and D of 1 m^2/s (b); with extension and Vi & Vo of 0.5 m/s and D of 1 m^2/s (c)

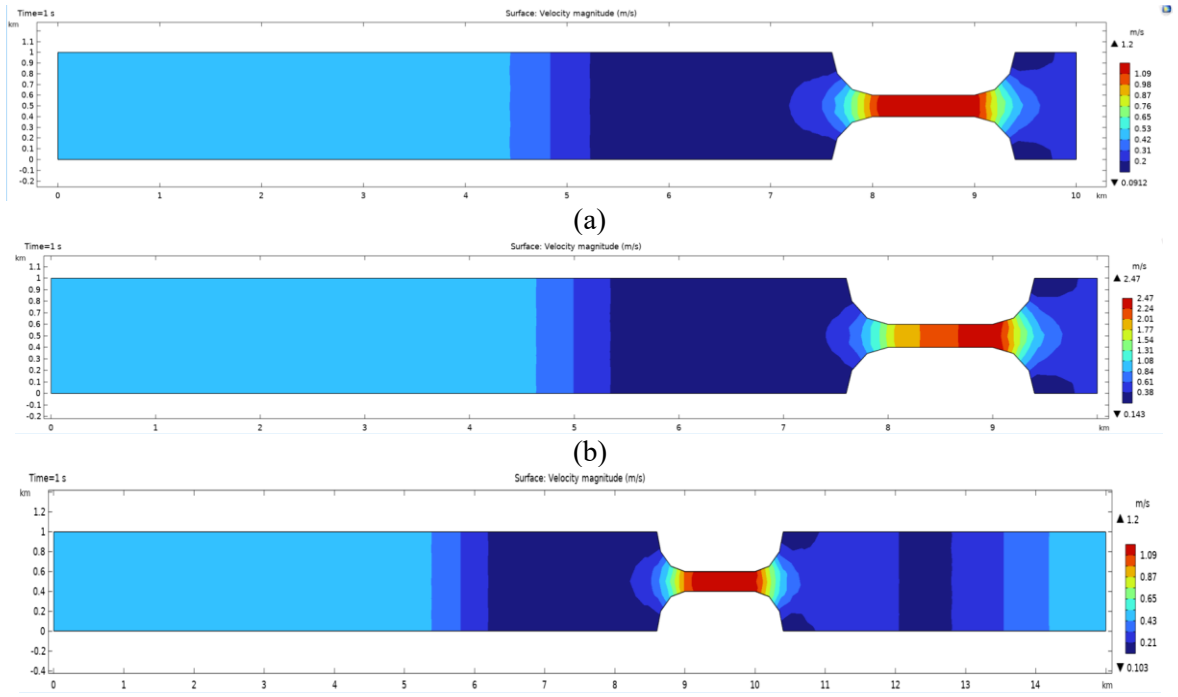

Figure 14. Velocity distribution for wide contraction geometry: Vi & Vo of 0.5 m/s and D of 1 m^2/s (a); Vi & Vo of 1 m/s and D of 1 m^2/s (b); With extension and Vi & Vo of 0.5 m/s and D of 1 m^2/s (c)

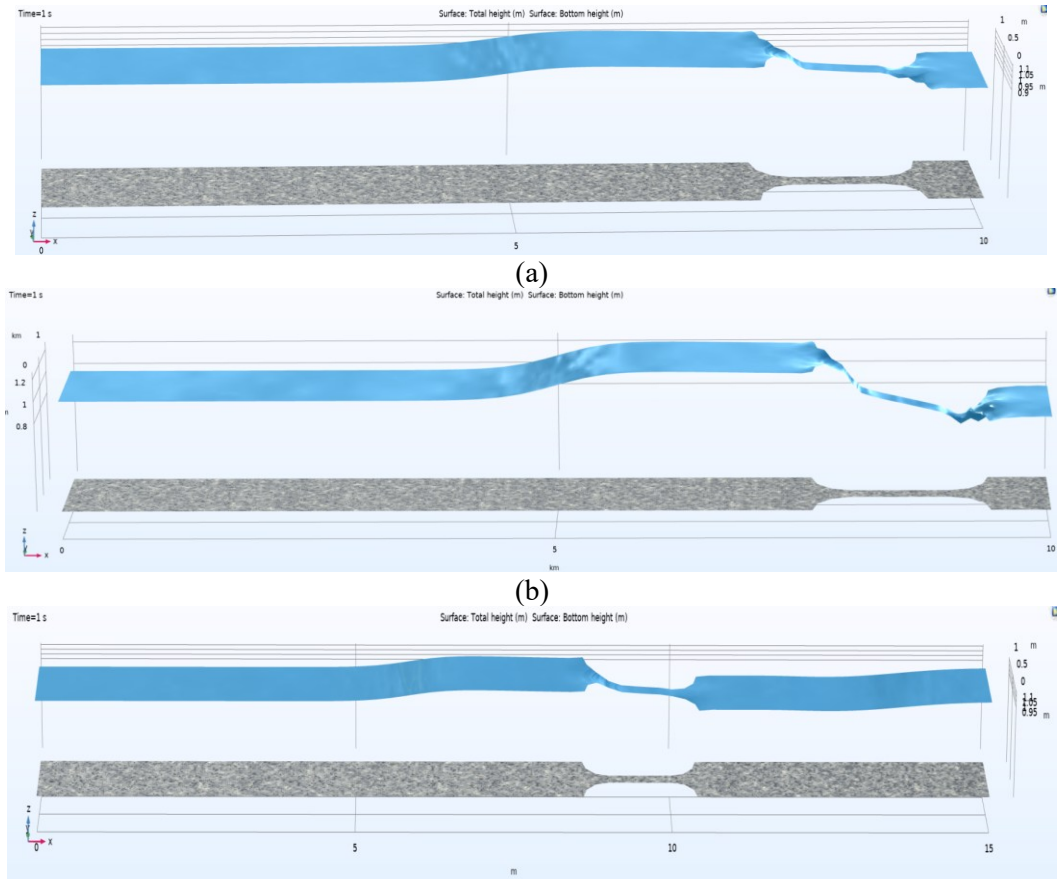

Figure 15. Height of free water surface for wide contraction geometry: Vi & Vo of 0.5 m/s andD of 1 m^2/s (a); Vi & Vo of 1 m/s and D of 1 m^2/s (b); with extension and Vi & Vo of 0.5 m/s and D of 1 m^2/s (c)

Comparing the figures that explain the velocities within the different contractions, it can be noticed that the two geometries: double semicircles (**Figure 12a**), and wide contraction (**Figure 14a**), provide high velocities which extend through a large area within the contraction compared to other geometries. **Figure 13** and **Figure 15** explain the free water surface of the corresponding figures.

The two geometries (double semicircles and a wide contraction) under the two scenarios of 1 m/s (**Figure 12b** and **Figure 14b**) and an additional 5 km extension (**Figure 12c** and **Figure 14c**) also produce a large high-velocity region compared with the corresponding other geometries. This velocity distribution maximises the convective phenomenon, thereby minimising saltwater intrusion. The increase in velocity can be explained as follows: since contractions reduce the cross-sectional area of flow, the depth of the free water surface before the contraction increases, producing backwater action that, in turn, increases velocity within the contraction. As a result, the upstream water level before the contraction will increase, causing an increase in flow velocity and a reduction in intrusion (see **Figure 9a–Figure 9c**, **Figure 11a–Figure 11c**, **Figure 13a–Figure 13c**, and **Figure 15a–Figure 15c**).

The proposed solution should consider specific conditions of each treated canal, such as ecological impacts, sediment dynamics, and navigation, which are also important in estuary rivers and canals. Since these conditions differ from one canal to another, the treatment should differ accordingly.

CONCLUSIONS

Seawater Intrusion SWI is a highly significant issue facing estuary rivers. The estuary cities are also affected by this problem. The published articles that have considered this problem can be divided into two groups. The first group considers estuary aquifers, while the second group considers estuary rivers. Many articles in these two groups focused on developing software or mathematical models to simulate saltwater intrusion. Only a few papers proposed a hydrodynamic solution to prevent the intrusion.

Considering this gap, this paper proposes a solution. The suggested solution includes constructing a contraction at the river's tail to minimise the intrusion. To assess the effectiveness of this solution, different contraction geometries were tested under three river-flow scenarios using COMSOL software. The tested geometries were: triangle, semicircle, double semicircle, and wide contractions. The three scenarios were: 1) under 0.5 m/s for inlet and outlet velocity, 2) under 1.0 m/s for inlet and outlet velocity, and 3) under 0.5 m/s for inlet and outlet velocity with a 5 km extension between the sea mouths and centres of contractions.

The results show that the best two contractions, producing the least intrusions, are double semicircles and wide contractions. The intrusions within a range of 60–120 mol/m3 concentrations for these two geometries were limited to 0.75 km beyond the contractions, under the conditions of 10 km and 1 km canal length and width, respectively, and an inlet and outlet velocity of 0.5 m/s and a diffusion coefficient of 1 m2/s. The tested contractions were assumed to be 0.4 km on each side, resulting in an 80% reduction in the cross-sectional area of the river. These two geometries are best for minimising intrusions because they produce high-velocity increments that extend over large regions within the contractions. Thus, the regions of these two contractions will increase convection, preventing saltwater from intruding upstream. However, before applying this solution to any river in practice, approvals from geologists and hydrologists concerning that river are required.

The planned future work in this field takes different directions. The first could be modelling a real river, using software and physical modelling. After approving the modelling approach, it can be applied to a real-scale river. Another aspect that could be considered in future studies concerns the influence of different sill shapes and heights (constructed on the canal bed) on the length of intrusion. A good result is expected from combining the contraction with the sill to reduce the intrusion, which is another gap that could be addressed in future work.

ACKNOWLEDGMENT

The authors would like to thank Anthony Pavlik for proofreading this article.

NOMENCLATURE

Symbols

a	acceleration	[m/s^2]
c	concentration of the species	[mol/m^3]
D	diffusion coefficient	[m^2/s]
J	mass flux diffusive flux	[mol/m^2·s]
p	pressure	[Pa]
R	reaction rate expression for the species	[mol/m^3·s]
t	time	[s]
u	velocity	[m/s]
Vi	inlet velocity	[m/s]
Vo	outlet velocity	[m/s]

Greek letters

ρ	density	[kg/m^3]
τ	viscous stress	[Pa]

Subscripts and superscripts

i	i-th species type

REFERENCES

1. Tian, Q., Gao, H., Tian, Y., Wang, Q., Guo, L., and Chai, Q., Attribution analysis and forecast of salinity intrusion in the Modaomen estuary of the Pearl River Delta, *Frontiers in Marine Science,* Vol. 11, 2024, https://doi.org/10.3389/fmars.2024.1407690.
2. Lin, Z., Zhang, G., Zou, H., and Gong, W., Salt intrusion dynamics in a well-mixed sub-estuary connected to a partially to well-mixed main estuary, *Ocean Science,* Vol. 20, No. 1, pp 181-199, 2024, https://doi.org/10.5194/os-20-181-2024.
3. Chen, Y., Xu, Y., Chen, G., Zeng, M., Zhang, T., Zhang, X., and Zhang, Y., Analysis of influencing factors of seawater intrusion in the Yangtze River Estuary and control for water supply security, *Frontiers in Marine Science,* Vol. 11, 2024, https://doi.org/10.3389/fmars.2024.1413548.
4. Ma, R., Qiu, C., Zhu, J., Zhang, Z., Zhu, Y., Kong, L., Ding, L., Qiu, W., and Wu, H., Dynamic cause of saltwater intrusion extremes and freshwater challenges in the Changjiang Estuary in flood season of 2022, *Frontiers in Marine Science,* Vol. 12, 2025, https://doi.org/10.3389/fmars.2025.1573883.
5. Dong, R., Cai, Y., Chen, X., Wang, C., and Lian, A., Ecological Risk Assessment of Saltwater Intrusion and Urban Ecosystem Management in Shenzhen City, *Land,* Vol. 13, No. 9, 1338, 2024, https://doi.org/10.3390/land13091338.
6. Perumal, M., Sekar, S., and Carvalho, P. C. S., Global Investigations of Seawater Intrusion (SWI) in Coastal Groundwaters in the Last Two Decades (2000–2020): A Bibliometric Analysis, *Sustainability,* Vol. 16, No. 3, 1266, 2024, https://doi.org/10.3390/su16031266.
7. Huang, H., Wang, Y., Wang, S., Lan, Y., and Huang, X., Saltwater Intrusion in the Changjiang River Estuary in Response to the East Route of the South-to-North Water Transfer Project in the New Period after 2003, *Sustainability,* Vol. 16, No. 2, 683, 2024, https://doi.org/10.3390/su16020683.

8. Hendrickx, G. G. and Pearson, S. G., On the Effects of Intertidal Area on Estuarine Salt Intrusion, *Journal of Geophysical Research: Oceans,* Vol. 129, No. 9, 2024, https://doi.org/10.1029/2023jc020750.
9. Wang, X., Shi, H., Cao, Y., Dong, C., and Li, C., Numerical Simulation of Saltwater Intrusion in the Yangtze River Estuary Based on a Finite Volume Coastal Ocean Model, *Journal of Marine Science and Engineering,* Vol. 12, No. 10, 1752, 2024, https://doi.org/10.3390/jmse12101752.
10. Xu, Z., Ma, J., and Hu, Y., Saltwater Intrusion Function and Preliminary Application in the Yangtze River Estuary, China, *International Journal of Environmental Research and Public Health,* Vol. 16, No. 1, 118, 2019, https://doi.org/10.3390/ijerph16010118.
11. Tao, Z., Chen, Y., Pan, S., Chu, A., Xu, C., Yao, P., and Rowley, S., The Influence of Wind and Waves on Saltwater Intrusion in the Yangtze Estuary: A Numerical Modeling Study, *Journal of Geophysical Research: Oceans,* Vol. 129, No. 9, e2024JC021076, 2024, https://doi.org/10.1029/2024JC021076.
12. Tomkratoke, S., Kongkulsiri, S., Narenpitak, P., and Sirisup, S., Drought and salinity intrusion in the Lower Chao Phraya River: Variability analysis and modeling mitigation approaches, *Hydrology and Earth System Sciences,* Vol. 29, No. 15, pp 3771-3793, 2025, https://doi.org/10.5194/hess-29-3771-2025.
13. Nguyen, H. D., Dang, D. K., and Bui, Q.-T., Estuary salinity prediction using machine learning: case study in the Hau estuary in Mekong River, Vietnam, *Water Supply,* Vol. 25, No. 2, pp 327-342, 2025, https://doi.org/10.2166/ws.2025.007.
14. Bich Thuc, P. T., Do, A. D., Trung, N. T., Nha Khanh, D. N., and Nam, N. T., Extent of Saltwater Intrusion and the Freshwater Exploitability in the Coastal Vietnamese Mekong Delta. A Case Study in Ham Luong estuary, *E3S Web of Conferences,* Vol. 626, 01004, 2025, https://doi.org/10.1051/e3sconf/202562601004.
15. Verri, G., De Lorenzis, A., Santos Da Costa, V., Sorolla, A., Löchner, A., Ribot, M., Marti, E., Delgado, S. C., Coppini, G., and Pinardi, N., Salt-wedge estuary's response to rising sea level, reduced discharge, and Nature-Based Solution, *Frontiers in Climate,* Vol. 6, 2024, https://doi.org/10.3389/fclim.2024.1408038.
16. Pokavanich, T. and Guo, X., Saltwater intrusion in Chao Phraya Estuary: A long, narrow and meandering partially mixed estuary influenced by water regulation and abstraction, *Journal of Hydrology: Regional Studies,* Vol. 52, 101686, 2024.
17. Menten, G., Melo, W., Pinho, J., Iglesias, I., and Antunes Do Carmo, J., Simulation of Saltwater Intrusion in the Minho River Estuary under Sea Level Rise Scenarios, *Water,* Vol. 15, No. 13, 2313, 2023, https://doi.org/10.3390/w15132313.
18. Zhu, S., Zhou, Z., Guo, Q., and Ma, J., A Study on the Cause of Layered Seawater Intrusion in the Daqing River Estuary of Liaodong Bay, China, *Sustainability,* Vol. 12, No. 7, 2842, 2020, https://doi.org/10.3390/su12072842.
19. Gao, C., Kong, J., Wang, J., and Chen, W., Nitrate fate in coastal unconfined aquifers influenced by preferential flows, *Frontiers in Marine Science,* Vol. 11, 2024, https://doi.org/10.3389/fmars.2024.1369869.
20. Truong, H.-D., Wang, S.-J., and Dang, M.-Q., Developing a coupled hydraulic-mechanical-chemical model to investigate the influences of geological model complexity in simulating seawater intrusion and land subsidence, *Journal of Hydrology,* Vol. 650, 132505, 2025.
21. Missimer, T. M. and Maliva, R. G., Salinity Barriers to Manage Saltwater Intrusion in Coastal Zone Aquifers During Global Climate Change: A Review and New Perspective, *Water,* Vol. 17, No. 11, 1651, 2025, https://doi.org/10.3390/w17111651.
22. Hendrickx, G. G., Manuel, L. A., Pearson, S. G., Aarninkhof, S. G. J., and Meselhe, E. A., An Earthen Sill as a Measure to Mitigate Salt Intrusion in Estuaries, *Estuaries and Coasts,* Vol. 47, No. 5, pp 1199-1208, 2024, https://doi.org/10.1007/s12237-024-01359-2.

23. COMSOL AB, *COMSOL Multiphysics Reference Manual, version 5.5.* Stockholm, Sweden, 2019, 1742.
24. Chanson, H., *The Hydraulics of Open Channel Flow: An Introduction*, Second ed. Elsevier Butterworth-Heinemann: Burlington, Massachusetts, 2004.
25. Xu, Z., Ma, J., Wang, H., Hu, Y., Yang, G., and Deng, W., River Discharge and Saltwater Intrusion Level Study of Yangtze River Estuary, China, *Water,* Vol. 10, No. 6, 683, 2018, https://doi.org/10.3390/w10060683.
26. Shaha, D. C., Cho, Y.-K., and Kim, T.-W., Effects of River Discharge and Tide Driven Sea Level Variation on Saltwater Intrusion in Sumjin River Estuary: An Application of Finite-Volume Coastal Ocean Model, *Journal of Coastal Research,* Vol. 287, pp 460-470, 2013, https://doi.org/10.2112/jcoastres-d-12-00135.1.
27. Ospino, S., Restrepo, J. C., Otero, L., Pierini, J., and Alvarez-Silva, O., Saltwater Intrusion into a River with High Fluvial Discharge: A Microtidal Estuary of the Magdalena River, Colombia, *Journal of Coastal Research,* Vol. 34, No. 6, 2018, https://doi.org/10.2112/jcoastres-d-17-00144.1.

APPENDIX

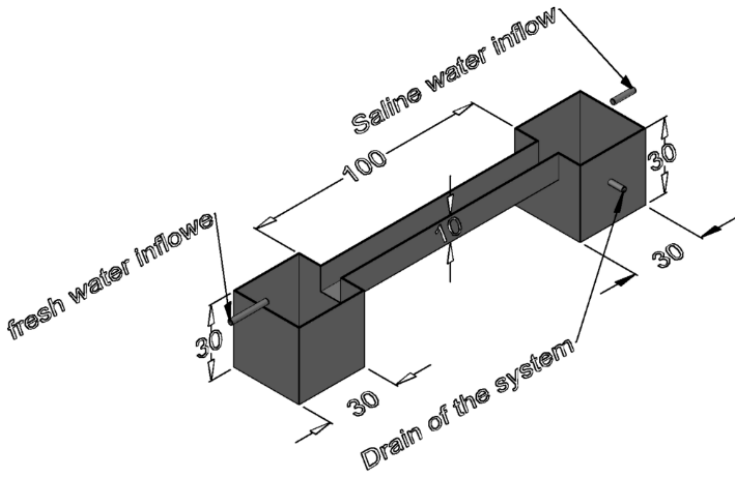

Figure A1. Physical modelling: AutoCAD design

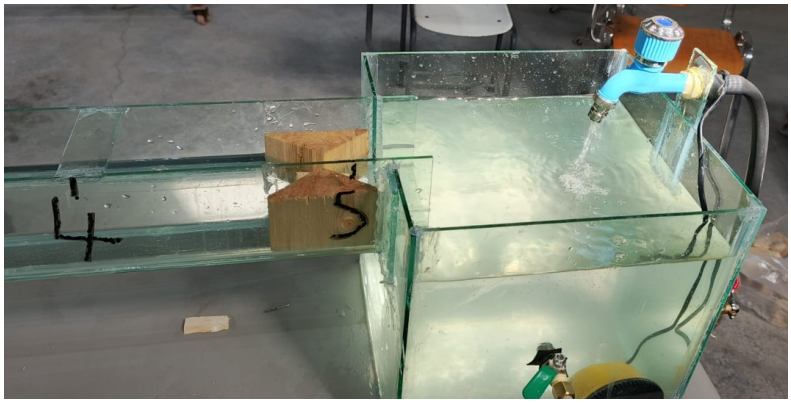

Figure A2. Physical modelling: triangle contraction

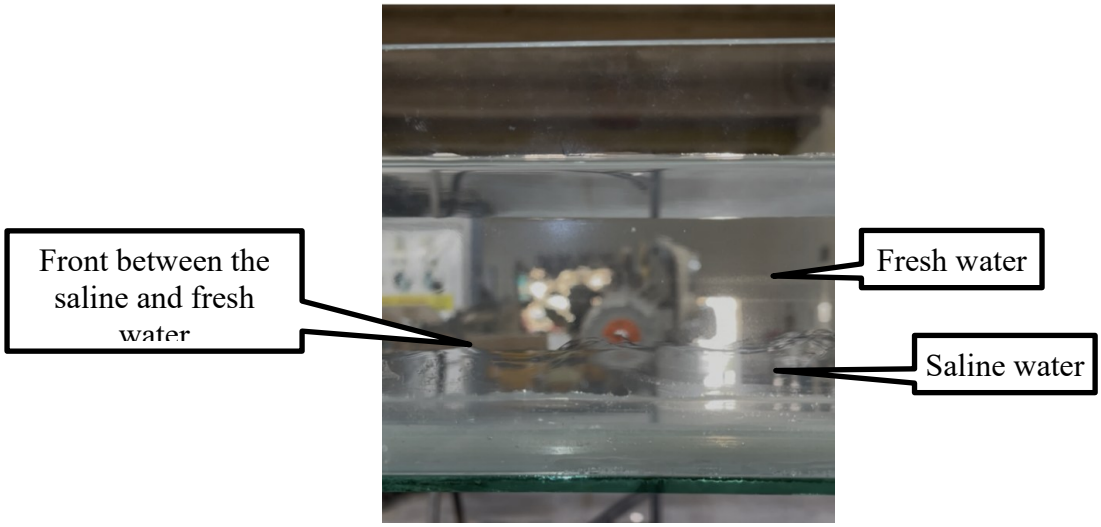

Figure A3. Physical modelling: stratification of saltwater intrusion in the canal

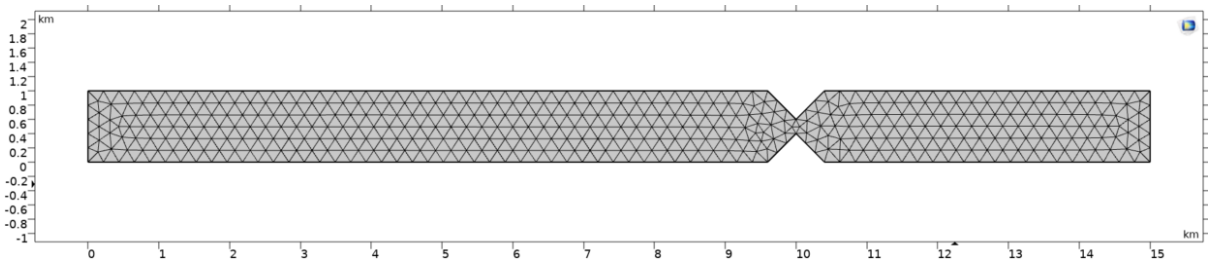

Figure A4. Triangle contraction with additional extension

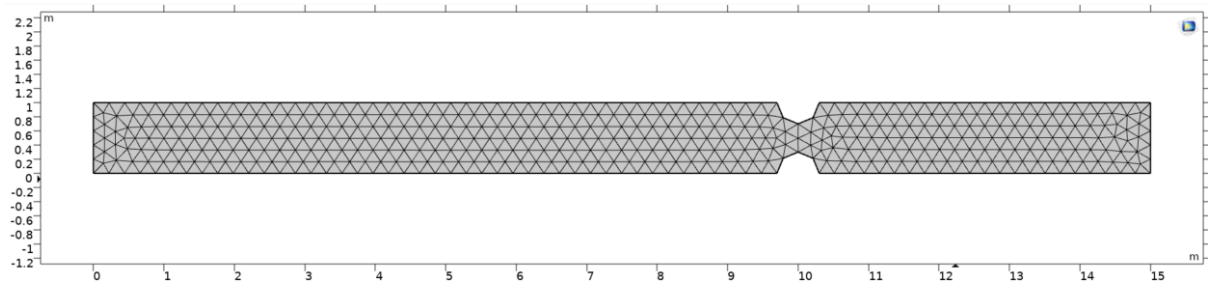

Figure A5. Semicircle contraction with additional contraction

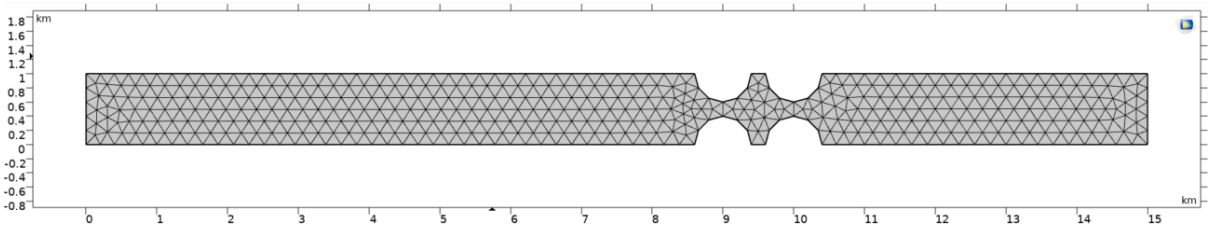

Figure A6. Double semicircles contraction with additional extension

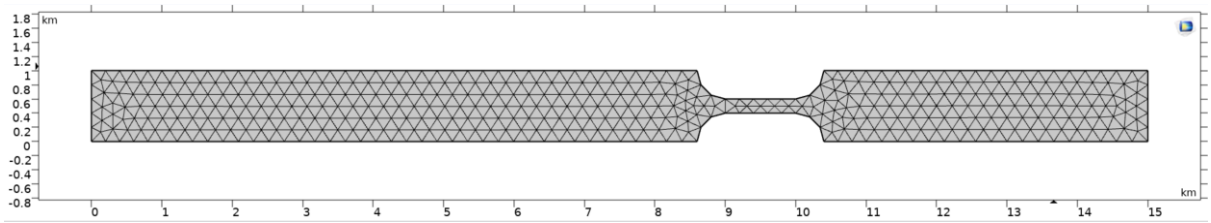

Figure A7. Wide contraction with additional extension

Paper submitted: 11.12.2025
Paper revised: 19.03.2026
Paper accepted: 22.03.2026